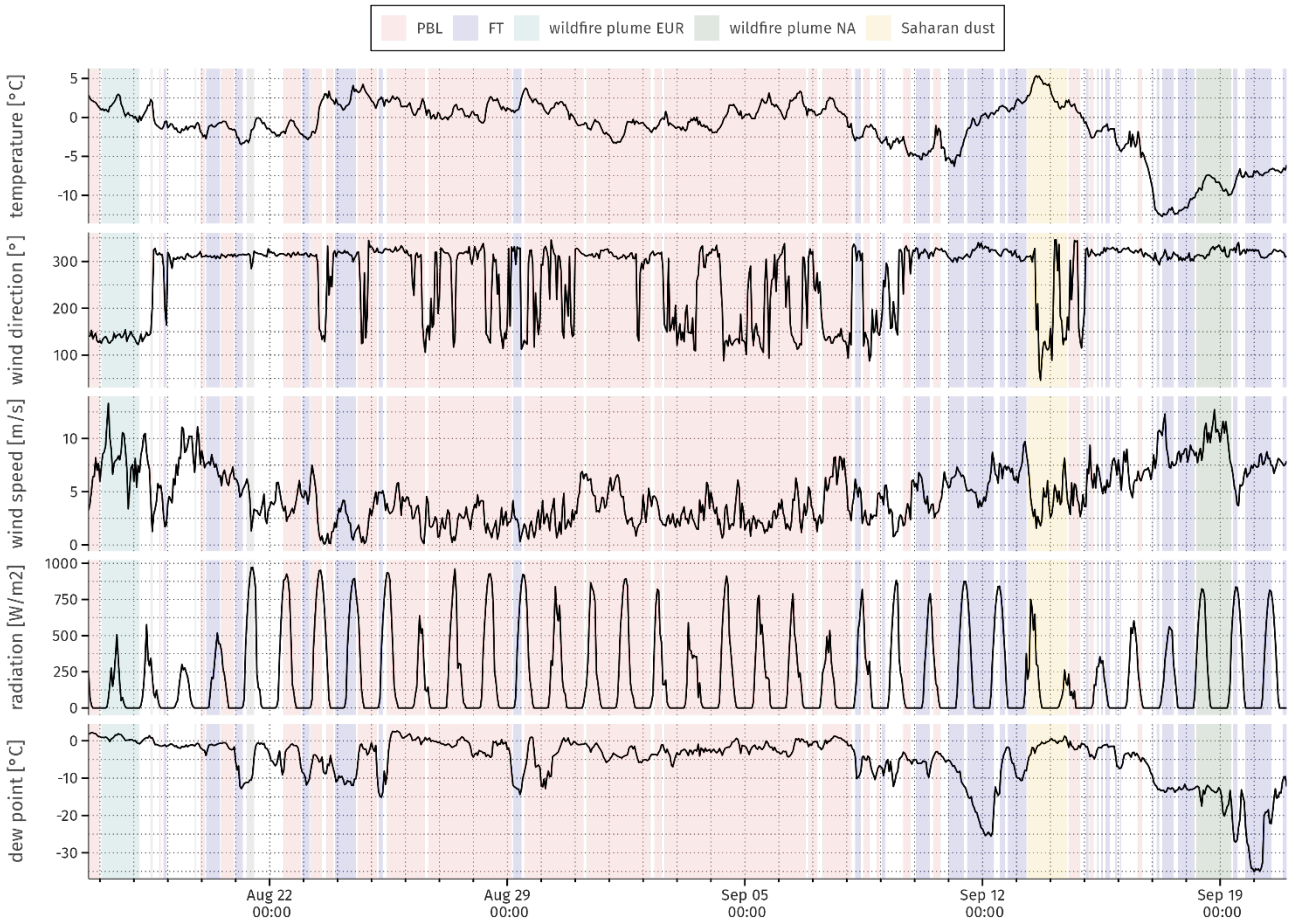
Supplement to:
Characterization of atmospheric carbon at a remote high-alpine site

Leïla Simon[1,*], Nora Nowak[1,*], Stephen J. Andrews[2,3], Michael Bauer[1,a], David M. Bell[1], Benjamin T. Brem[1], Fabrizia Cavalli[8], Rico K.Y. Cheung[1,b], Zachary C.J. Decker[1,c,d], Jim R. Hopkins[2,3], Christoph Hüglin[7], Matic Ivančič[4], Alejandro Keller[5], Gašper Lavrič[4], Thierry Léonardis[6], Robin Modini[1], Jean-Philippe Putaud[8], Stefan Reimann[7], Martin Rigler[4], Thérèse Salameh[6], Martin Steinbacher[7], Martin K. Vollmer[7], Ernest Weingartner[5], Martin Gysel-Beer[1]

[1]PSI Center for Energy and Environmental Sciences, Villigen PSI, 5232, Switzerland
[2]Wolfson Atmospheric Chemistry Laboratories, The University of York, York YO10 5DD, United Kingdom
[3]National Centre for Atmospheric Science, The University of York, York YO10 5DD, United Kingdom
[4]Aerosol Magee Scientific, Kamniška 39A, Ljubljana, 1000, Slovenia
[5]Institute for Sensors and Electronics, University of Applied Sciences Northwestern Switzerland, Windisch, 5210, Switzerland
[6]IMT Nord Europe, Institut Mines-Télécom, Université Lille, Centre for Energy and Environment, Lille, 59000, France
[7]Laboratory for Air Pollution/Environmental Technology, Empa, Dübendorf, 8600, Switzerland
[8]European Commission, Joint Research Centre (JRC), Ispra, 21027, Italy
[a]now at: Aerosol Chemistry Department, Max Planck Institute for Chemistry, 55128 Mainz, Germany
[b]now at: Department of Environmental Sciences, University of Basel, Basel, 4056, Switzerland
[c]now at: Environmental Defense Fund, Boulder, CO, 80302, USA
[d]now at: Cooperative Institute for Research in Environmental Sciences, University of Colorado Boulder, Boulder, CO 80309, USA
[*]These authors contributed equally to this work

Correspondence to: Leïla Simon (leila.simon@psi.ch) and Martin Gysel-Beer (martin.gysel@psi.ch)



25

Figure S1: Meteorological conditions at JFJ during the campaign.

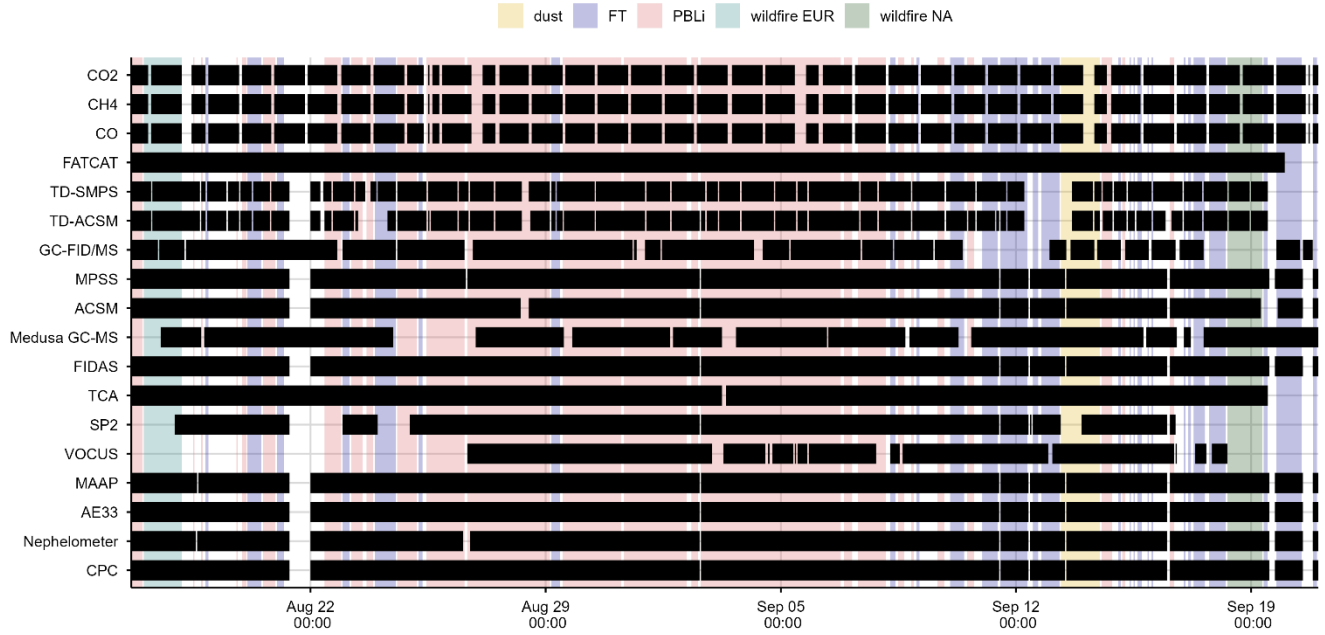


Figure S2: Data coverage of the different instruments during the campaign. Due to a fossil fuel contamination event on August 21st, data was removed for the TD-SMPS, TD-ACSM, FIDAS, SP2, MAAP, AE33, Nephelometer and CPC.

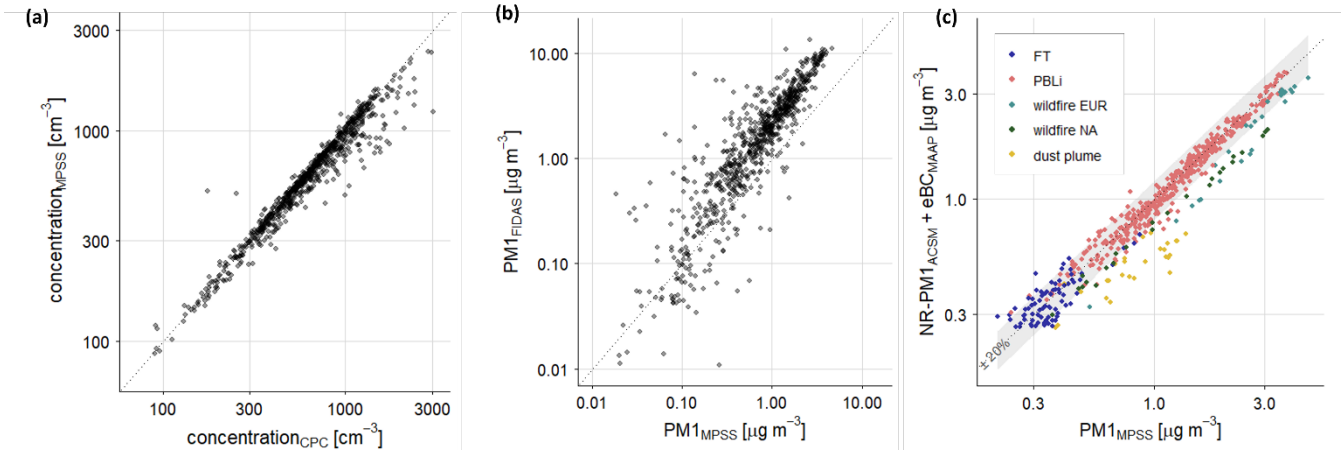


Figure S3: Aerosol instrument comparisons. (a) Comparison of total aerosol number concentrations measured by CPC and MPSS. (b) Comparison of PM_1 mass concentrations measured by MPSS and FIDAS (linear regression: y=2.4x, R^2=0.91). The MPSS values are calculated from number size distribution measurements assuming spherical particles with a density calculated using the density and the time-dependent relative proportion of the PM1 constituents (avg of 1.4 g cm^{-3}) and the FIDAS data are the default PM_1 output by the instrument firmware. (c) Comparison of PM_1 mass concentrations measured by MPSS and ToF-ACSM + MAAP. The observed deviations during the dust and wildfire periods could be due to different sizes (these particles are larger and might be missed by the ACSM due to the lens transmission cut-off), different composition (the ACSM is not calibrated for organic aerosol) and different absorption properties (which would make the eBC measurements less reliable). For (c), data was filtered to only cover PM_1 >3 times the sum of LODs for ACSM. Data in this figure was averaged hourly.

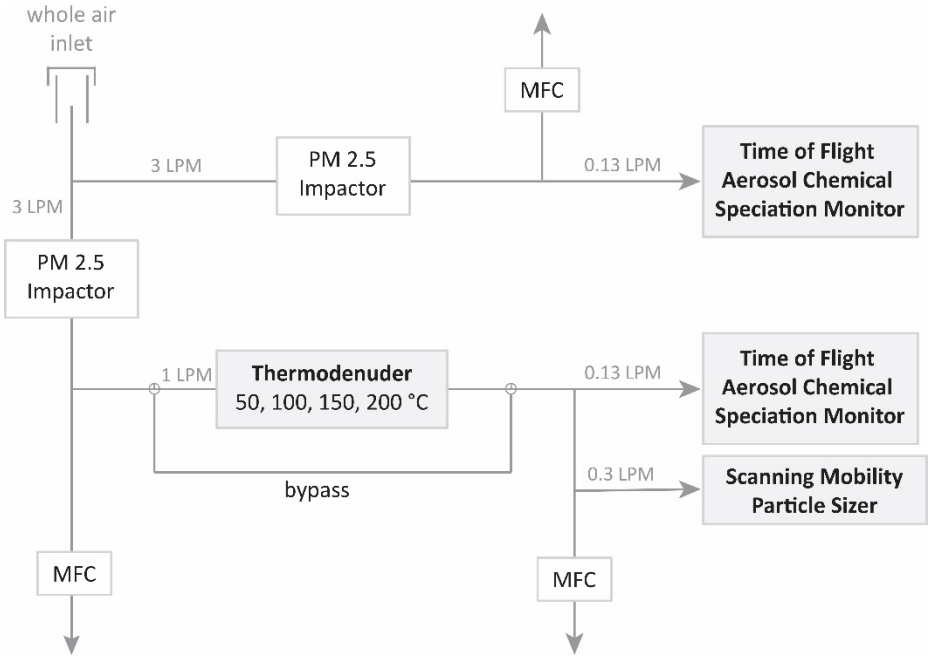


Figure S4: Thermodenuder-setup for aerosol volatility measurements. MFC = mass flow controller

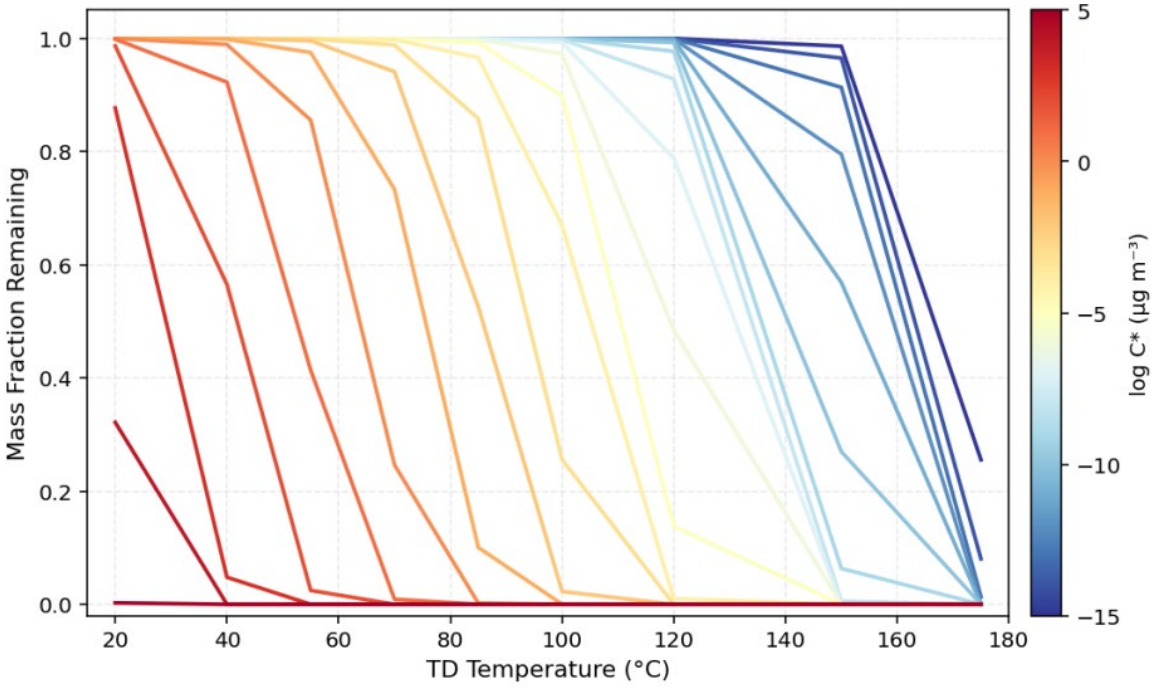


Figure S5: Modelled mass fraction remaining from log10 *C -15 to +5, based on the thermodenuder temperature, for a diameter of 150 nm assuming a log normal size distribution with a geometric standard deviation of 2.**

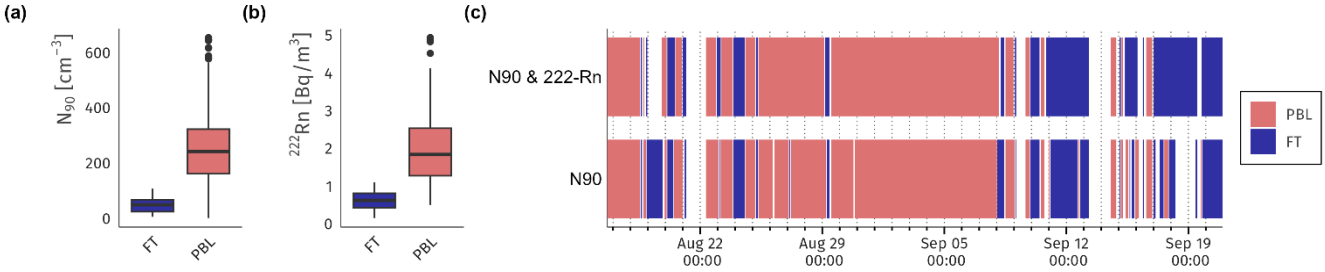


Figure S6: PBL and FT were distinguished based on a combined criterion of N90 and 222Rn signals (resulting boxplots shown in (a) and (b). (c) Timeseries of this classification, as well as one based on N90 only (where N90 ≥ 83 cm^{-3} is defined as PBL conditions).

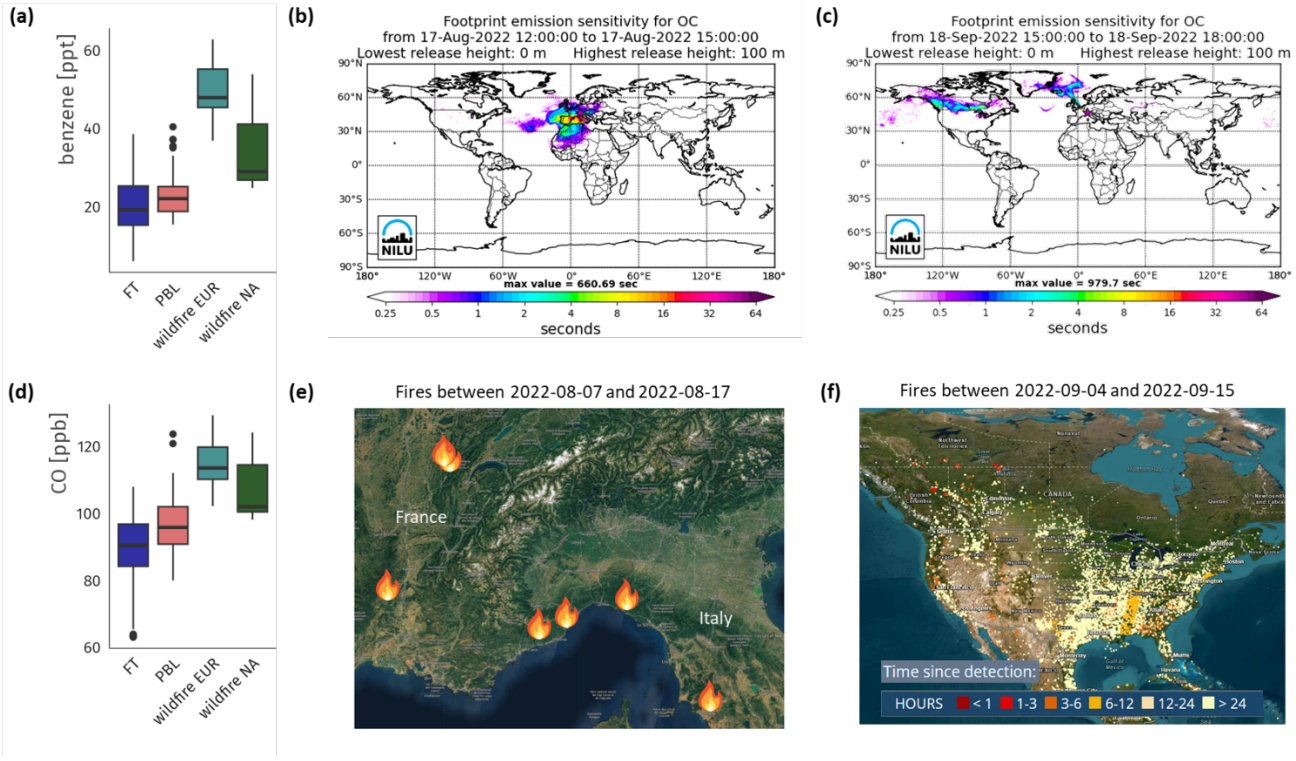


Figure S7: Wildfire plumes were identified by considering gaseous enhancements of benzene and CO concentrations, as well as source fingerprints and inventories. (a) Benzene and (d) CO concentrations for different air mass types (including wildfire plumes) (b) and (c) present examples of emissions sensitivity footprints for the dates of the wildfire plumes, while (e) and (f) present fire reports for periods matching the two wildfire plumes.

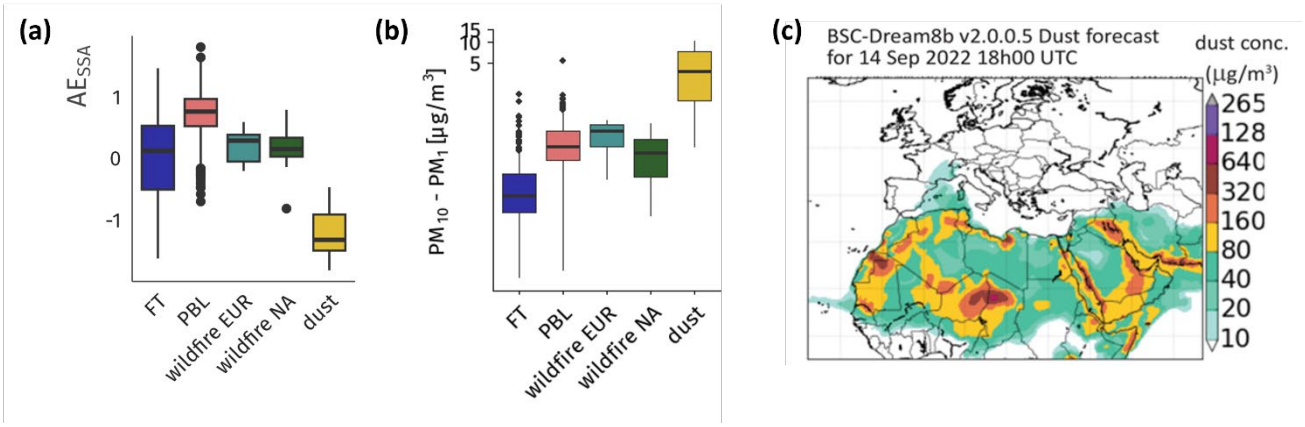


Figure S8: A Saharan dust plume was identified based on the concentration of coarse mode particles and of a negative Angstrom exponent of the single scattering albedo, as well as dust forecast. (a) presents the Angstrom exponent of the single scattering albedo (AE_{SSA}) and (b) the coarse mode particle concentration (PM_{10}-PM_1) for the different air masses (including dust). (c) shows the dust forecast for the dust event observed during the campaign.

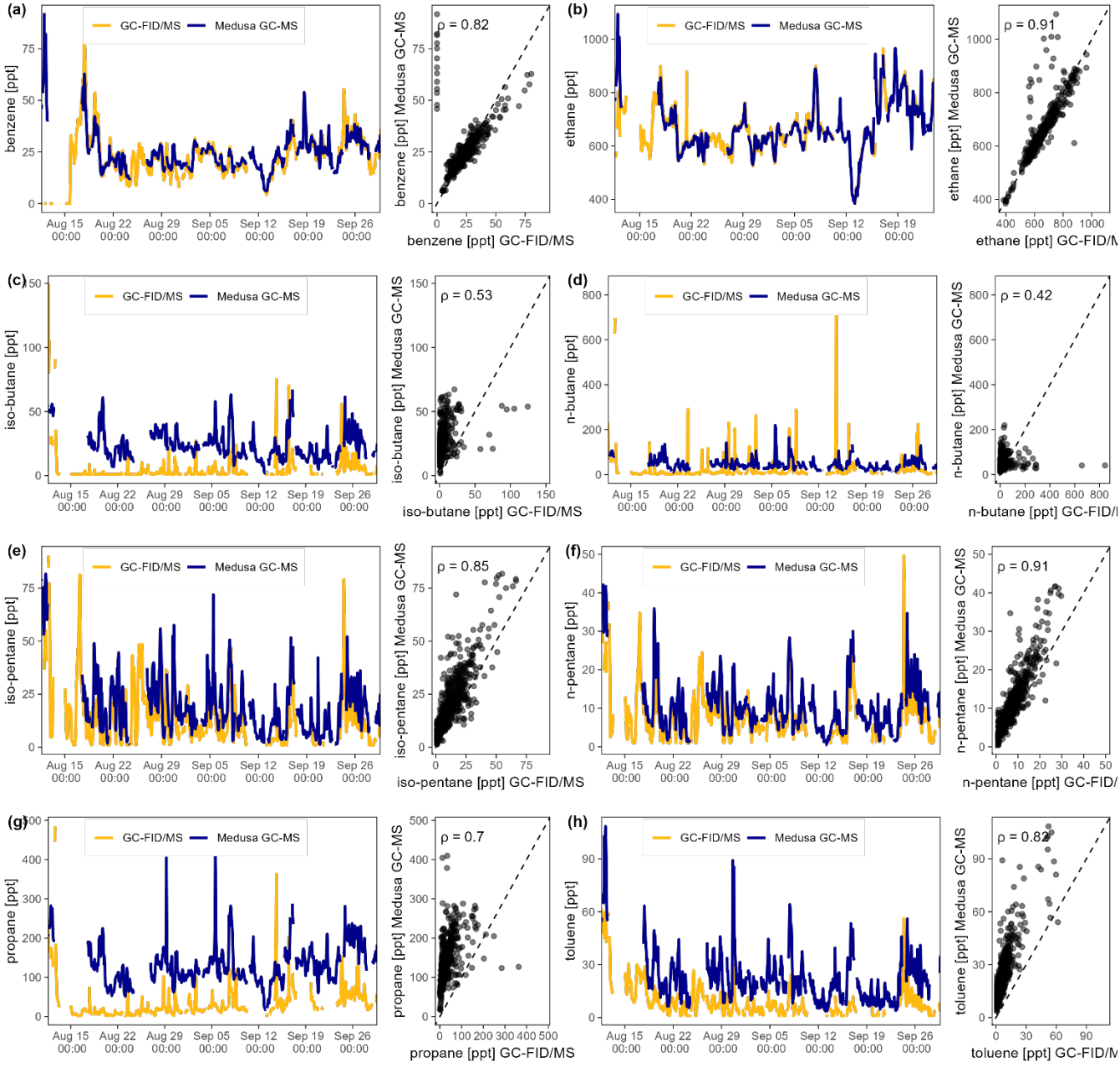


Figure S9: Compounds measured with both GC-instruments.

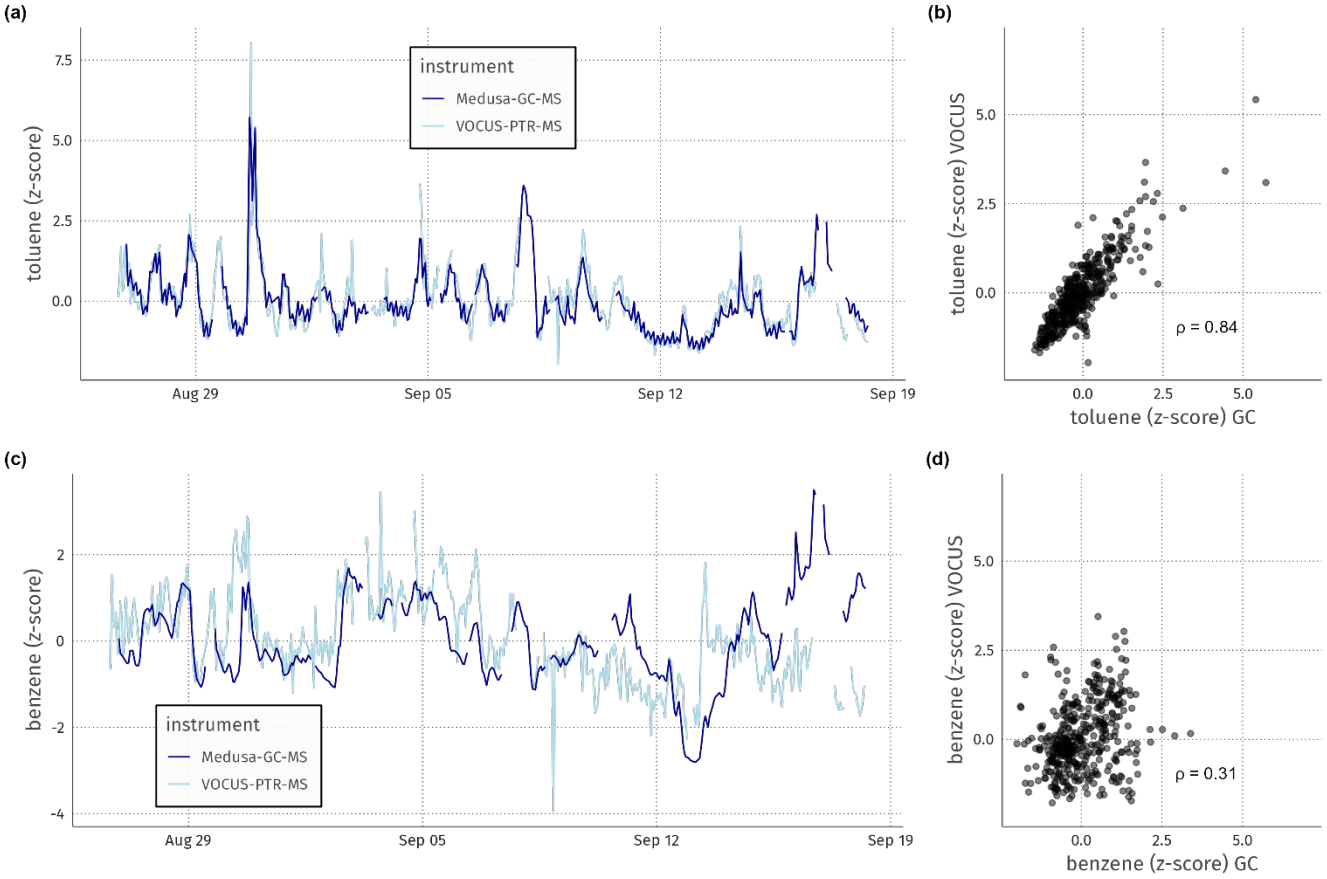


Figure S10: Temporal variability of the z-score (number of standard deviations by which each value is above or below the mean) of toluene and benzene measured by Vocus PTR-MS and Medusa-GC-MS.

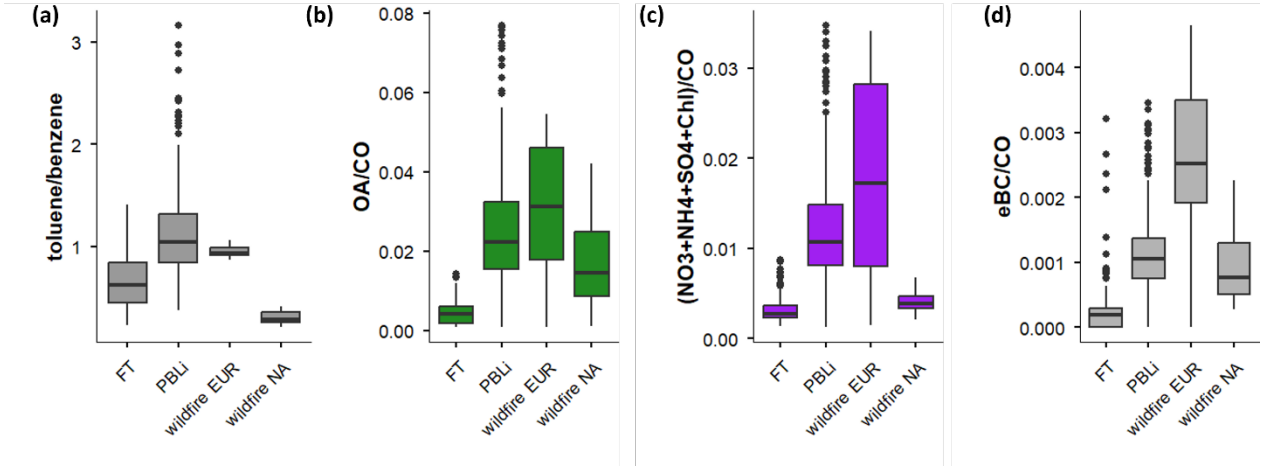


Figure S11: Boxplots of (a) toluene/benzene, (b) OA/CO, (c) inorganic NR-PM$_1$ (inorg.)-to-CO ratio and (d) eBC/CO for the different air masses

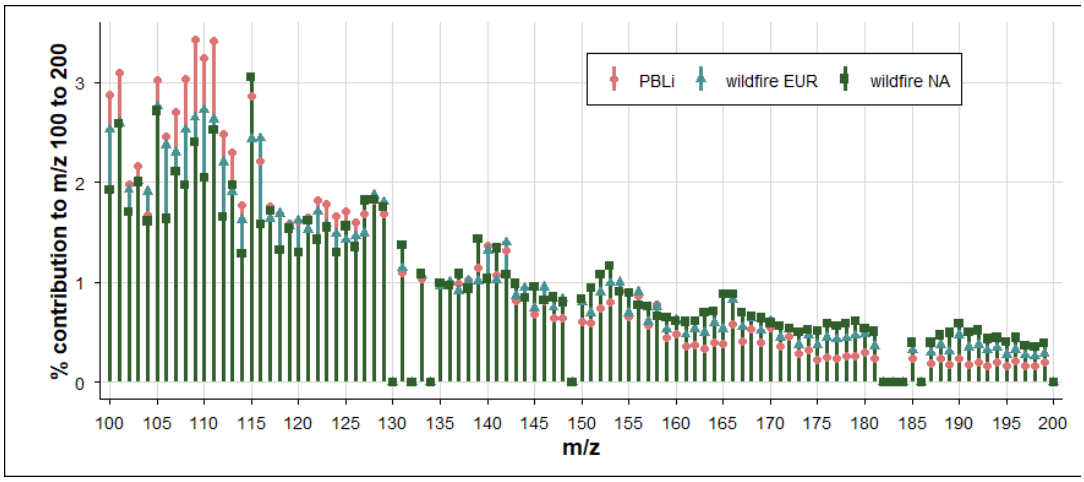


Figure S12: Contribution of m/z 100 to 200 to the sum of these m/z for the air masses PBLi, wildfire EUR and wildfire NA.

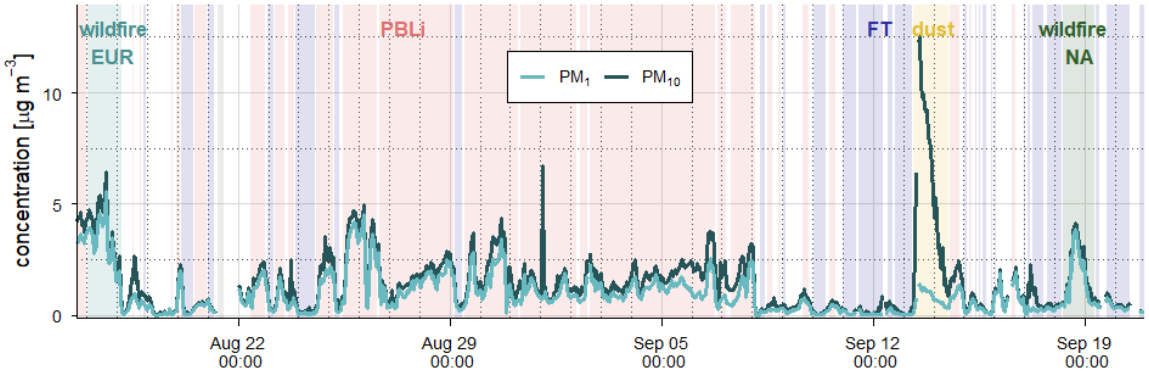


Figure S13: Temporal variability of PM_1 and PM_{10} as default outputs by the instrument firmware measured by FIDAS during the campaign (scaled to MPSS by a factor of 2.4).

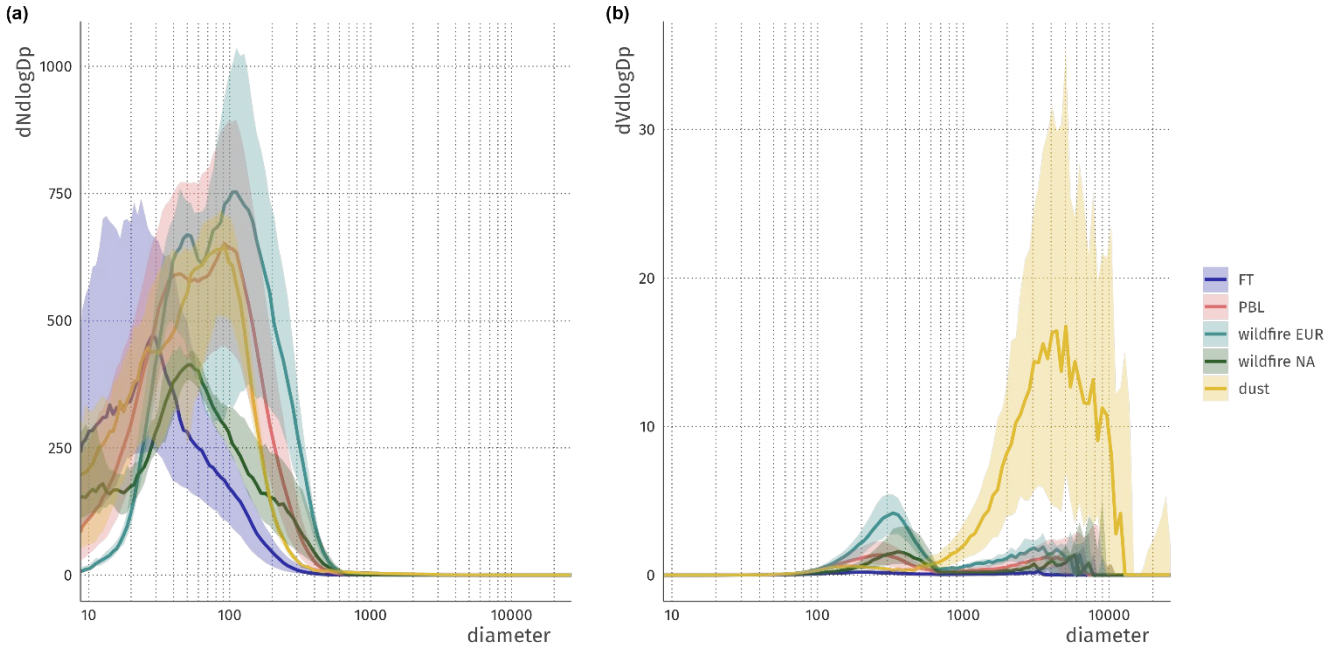


Figure S14: Particle size distributions averaged by air mass type (shaded areas indicate 25th to 75th percentile of the data). (a) Number size distributions (b) Volume size distributions. The size distributions from MPSS and Fidas were merged; for the MPSS, diameters to 650 nm included were used, and for diameters above 650 nm the Fidas data was used.

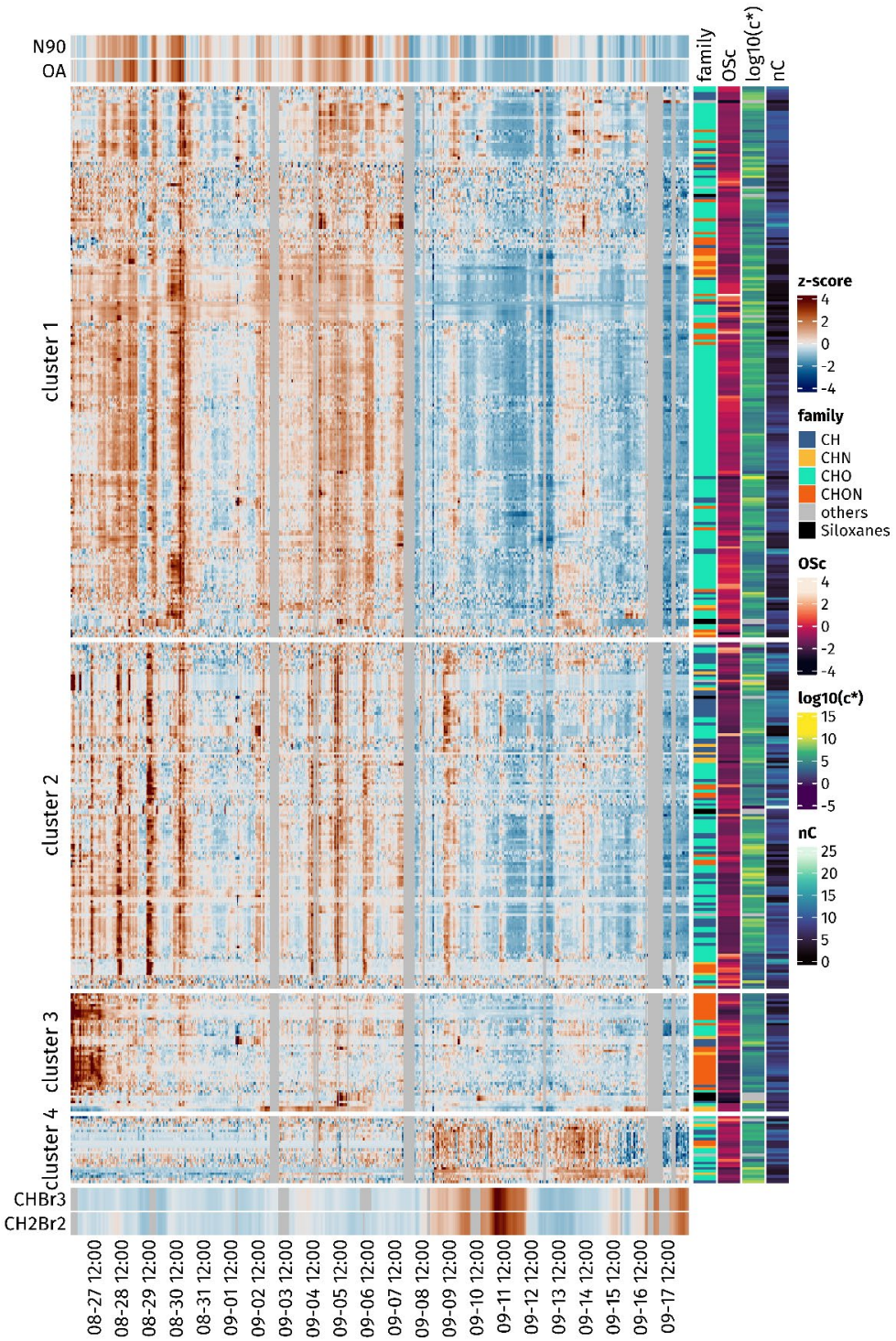


Figure S15: Heatmap of time series of ions detected by VOCUS-PTR-MS. CHBr3 and CH2Br2 were measured with the Medusa-GC-MS.

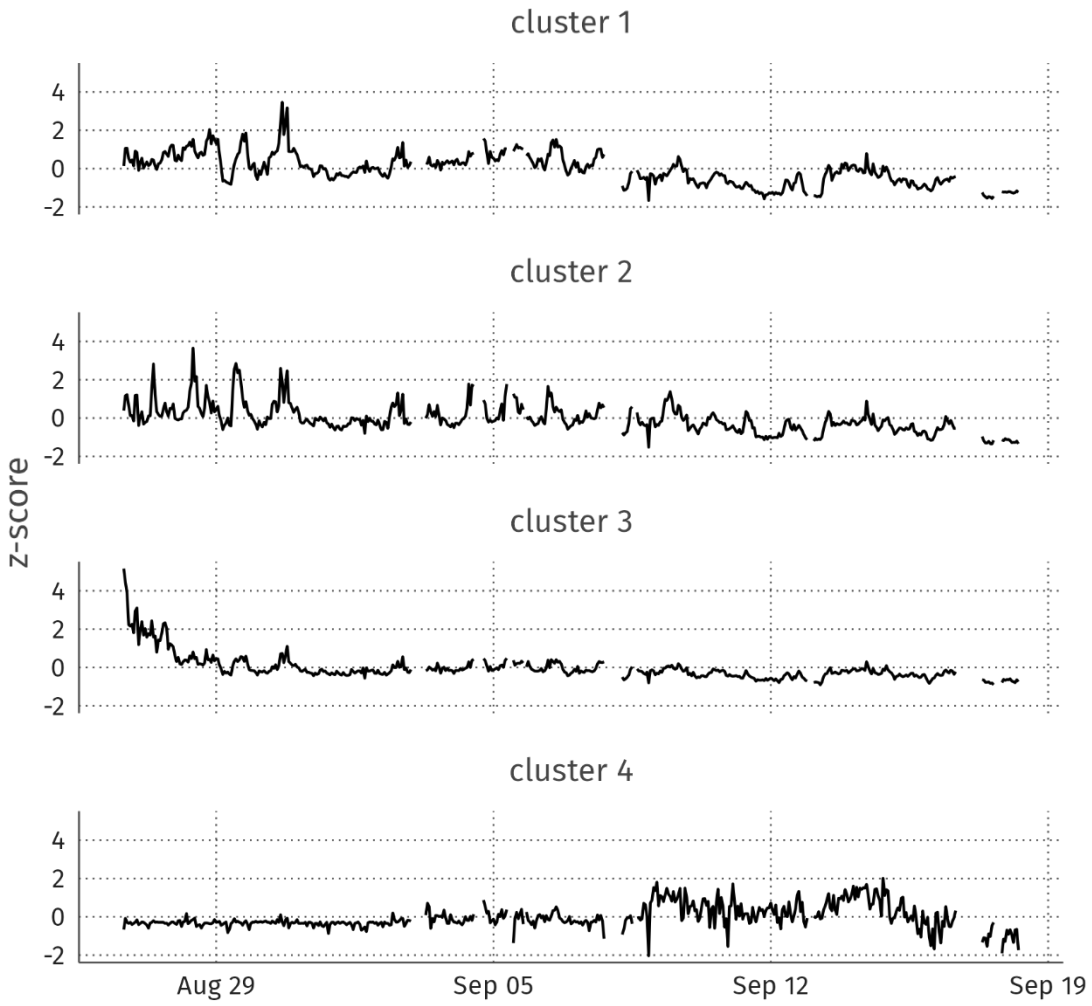


Figure S16: Representative temporal profiles of VOCUS-PTR signal clusters derived from shape-based clustering.

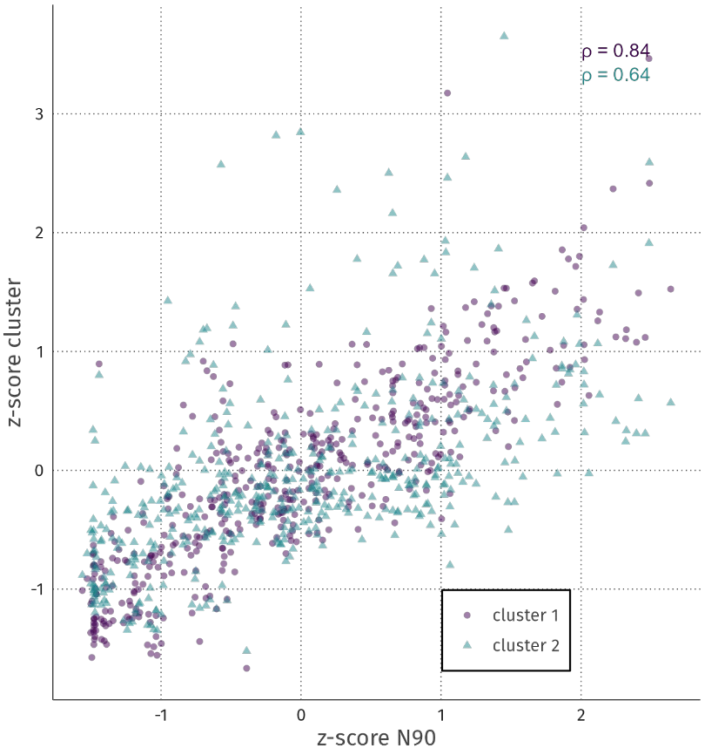


Figure S17: Correlation between relative changes of N90 and VOCUS clusters 1 and 2.

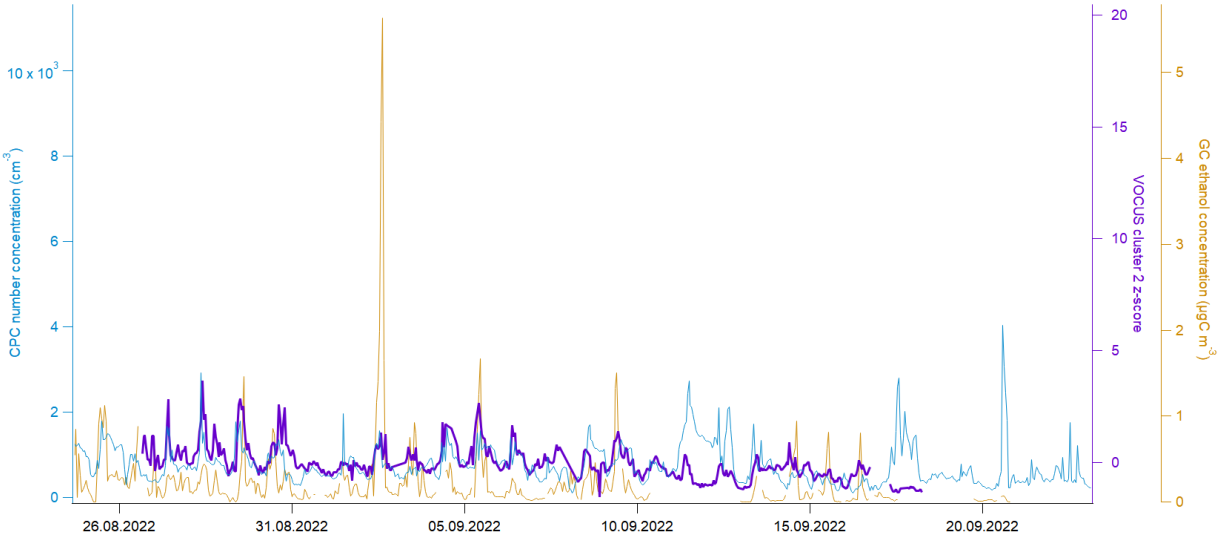


Figure S18: Timeseries of the number concentration measured by the CPC, the VOCUS Cluster 2 and ethanol measured by the GC-FID/MS

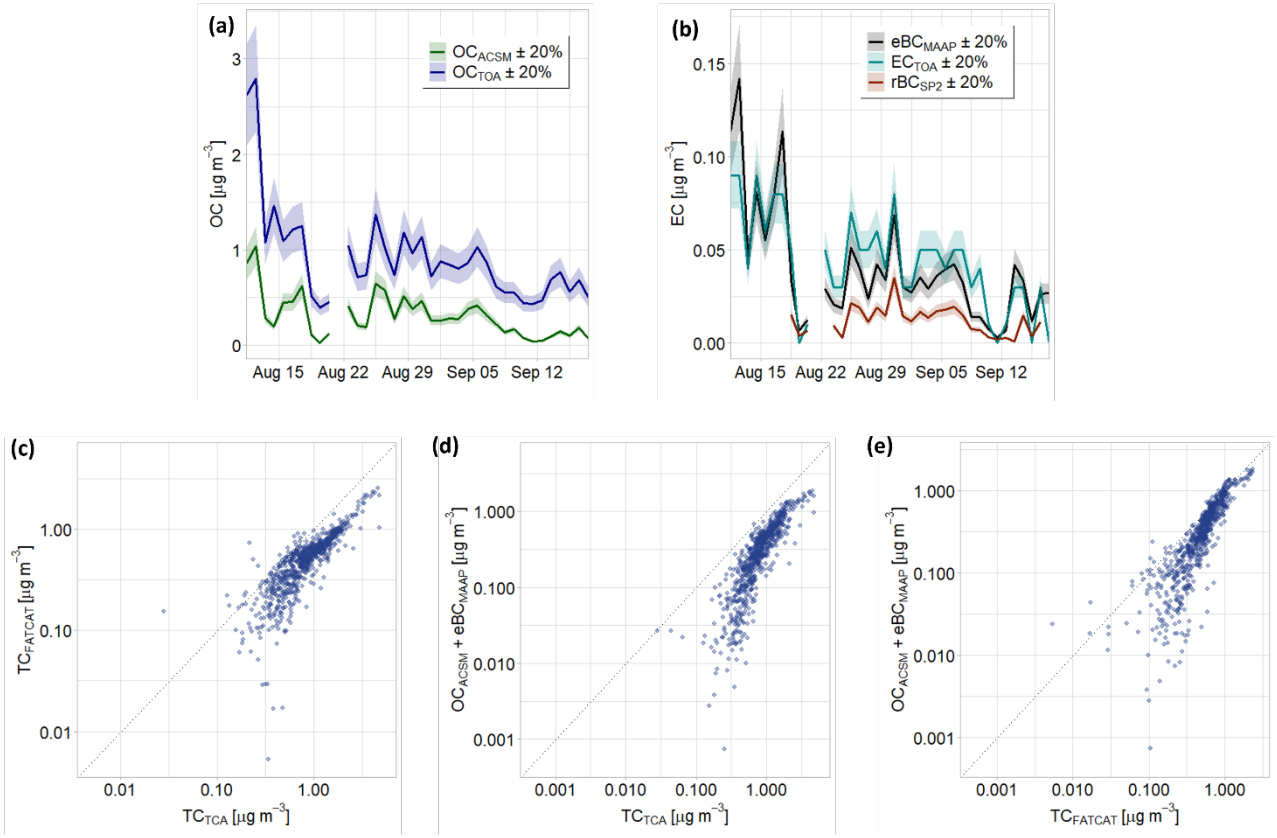


Figure S19: Total carbon closure on daily time resolution (for online instruments, the data was daily averaged). (a) Time series of daily averages of OC concentrations derived from OA (ACSM) and OC concentrations obtained from thermo-optical measurements. (b) Time series of daily averages of EC concentrations as eBC from MAAP, rBC from SP2 and EC from thermo-optical measurements. (c) Scatter plot of total carbon from FATCAT vs TCA (linear regression model: y=0.54x, R^2=0.95). The FATCAT data, which has an original time resolution of 2h, was resampled to 1h. (d) Scatter plot of total carbon from ACSM+MAAP vs TCA (linear regression model: y=0.42x, R^2=0.91). (e) Scatter plot of total carbon from ACSM+MAAP vs FATCAT (linear regression model: y=0.76x, R^2=0.93).

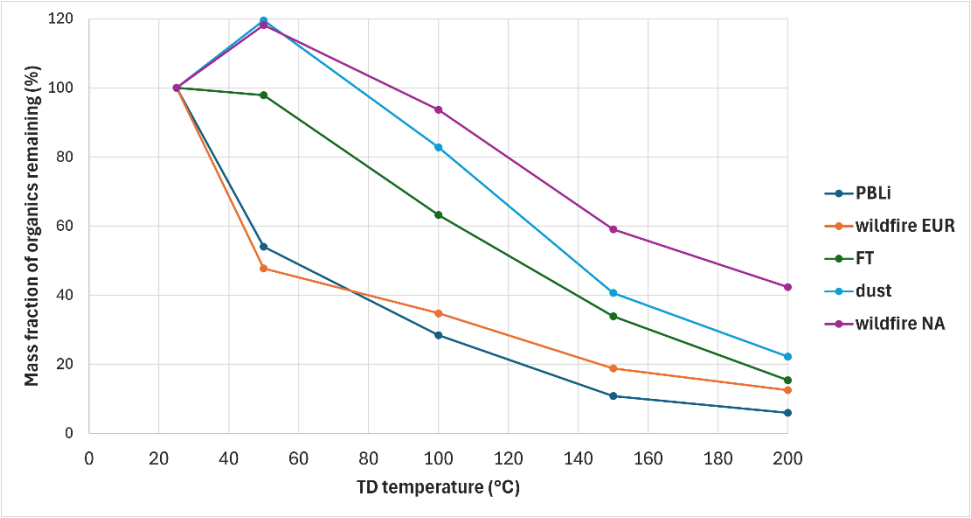


Figure S20: Averaged volatility profiles of OA measured by the TD-ACSM for the different air masses (PBLi, wildfire EUR, FT, dust and wildfire NA)

105

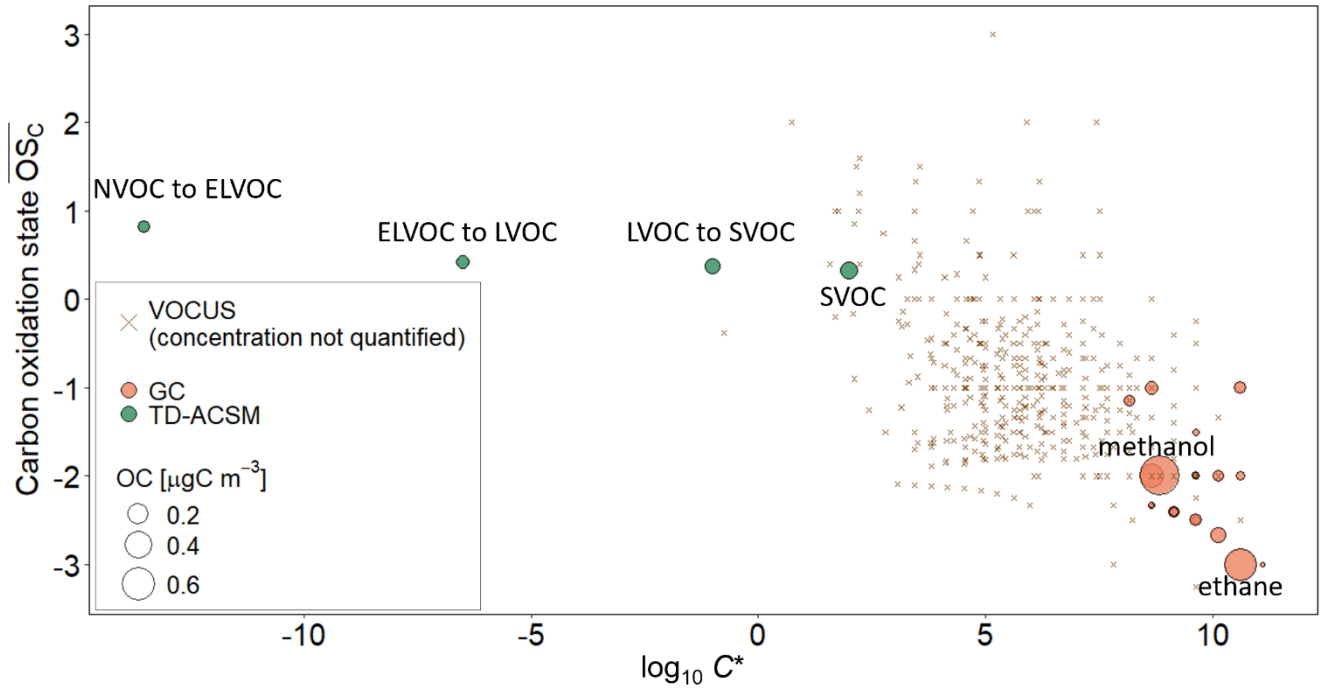


Figure S21: Carbon oxidation state (OSc) vs volatility ($\log_{10}$ *C) for organic carbon measured in both gas and particle phase by the GCs, the Vocus and the TD-ACSM at 298-300 K.**

Table S1: Speciated and quantified VOCs using the GC-FID/MS and the Medusa-GC-MS. Averaged VMR (pptC) over the whole campaign is indicated, as well as the VOC families the compounds were assigned to.

Industry name	Instrument	Mean VMR (pptC)	Family
acetylene	GC-FID/MS	125.65	alkynes
but-1-ene	GC-FID/MS	21.81	alkenes
buta-1,3-diene	GC-FID/MS	12.81	alkenes
cis-2-butene	GC-FID/MS	11.39	alkenes
ethanol	GC-FID/MS	719.54	alcohols
ethene	GC-FID/MS	48.99	alkenes
methanol	GC-FID/MS	2276.57	alcohols
methyl-2-pentane	GC-FID/MS	20.79	alkanes
n-hexane	GC-FID/MS	10.51	alkanes
propene	GC-FID/MS	79.15	alkenes
trans-2-butene	GC-FID/MS	9.43	alkenes
C4F10	Medusa	0.87	halogenated
C6F14	Medusa	2.03	halogenated
CCl4	Medusa	74.63	halogenated
CF4	Medusa	89.1	halogenated
CFC-113	Medusa	136.9	halogenated
CFC-114	Medusa	32.71	halogenated
CFC-115	Medusa	17.68	halogenated
CFC-11	Medusa	219.01	halogenated
CFC-13	Medusa	3.36	halogenated
CH2Br2	Medusa	0.82	halogenated
CH2Cl2	Medusa	58.76	halogenated
CH3Br	Medusa	6.73	halogenated
CH3CCl3	Medusa	2.33	halogenated
CH3Cl	Medusa	530.86	halogenated
CH3I	Medusa	0.4	halogenated
CHBr3	Medusa	0.75	halogenated
CHCl3	Medusa	9.94	halogenated
COS	Medusa	482.03	others
H-1211	Medusa	3.04	halogenated
H-1301	Medusa	3.4	halogenated
H-2402	Medusa	0.78	halogenated
HCFC-124	Medusa	1.83	halogenated
HCFC-133a	Medusa	1.1	halogenated

HCFC-141b	Medusa	51.88	halogenated
HCFC-22	Medusa	257.88	halogenated
HFC-1233zdE	Medusa	0.73	halogenated
HFC-1234yf	Medusa	0.73	halogenated
HFC-1234zeE	Medusa	0.79	halogenated
HFC-125	Medusa	90.17	halogenated
HFC-134a	Medusa	271.03	halogenated
HFC-143a	Medusa	62.31	halogenated
HFC-152a	Medusa	19.63	halogenated
HFC-227ea	Medusa	7.02	halogenated
HFC-236fa	Medusa	0.76	halogenated
HFC-23	Medusa	36.54	halogenated
HFC-245fa	Medusa	11.74	halogenated
HFC-32	Medusa	40.52	halogenated
HFC-41	Medusa	0.5	halogenated
HFC-4310mee	Medusa	1.62	halogenated
PCE	Medusa	3.77	halogenated
PFC-116	Medusa	10.45	halogenated
PFC-218	Medusa	2.29	halogenated
PFC-318	Medusa	8.23	halogenated
TCE	Medusa	0.09	halogenated
desflurane	Medusa	1.04	halogenated
isoflurane	Medusa	0.46	halogenated
sevoflurane	Medusa	36.32	halogenated
benzene	both (mean)	141.34	aromatics
ethane	both (mean)	1330.72	alkanes
iso-butane	both (mean)	53.08	alkanes
iso-pentane	both (mean)	82.6	alkanes
n-butane	both (mean)	129.46	alkanes
n-pentane	both (mean)	45.74	alkanes
propane	both (mean)	224.16	alkanes
toluene	both (mean)	102.45	aromatics

Text S1: Formulas for the calculation of the probability of the sampled air to be of FT or PBL origin.

The following formulas were established by Brunner et al. (2021).

Probability of the sampled air to be of free tropospheric origin (P_{FT}):

$$P_{FT} = \frac{PDF_{FT}}{PDF_{FT} + PDF_{PBL}} \frac{1}{1 + e^{k(N_{90} - N_{90,th})}}$$

With PDF_{FT} the probability density function of ^{222}Rn in the FT:

$$PDF_{FT} = \frac{1}{\sigma_{FT}\sqrt{\pi}} e^{-\frac{1}{2}(\frac{log_{10}(Rn) - \mu_{FT}}{\sigma_{FT}})^2}$$

And PDF_{PBL} the probability density function of ^{222}Rn in the PBL:

$$PDF_{PBL} = \frac{1}{\sigma_{PBL}\sqrt{\pi}} e^{-\frac{1}{2}(\frac{log_{10}(Rn) - \mu_{PBL}}{\sigma_{PBL}})^2}$$

Where $N_{90,th}$ = 120 cm^{-3}, k = 0.1, μ_{FT} = -0.139 Bq/std m^{-3}, σ_{FT} = 0.239 Bq/std m^{-3}, μ_{PBL} = 0.403 Bq/std m^{-3}, σ_{PBL} = 0.238 Bq/std m^{-3}, Rn concentrations are in Bq/std m^{-3}

Bibliography:

Brunner, C., Brem, B.T., Collaud Coen, M., Conen, F., Hervo, M., Henne, S., Steinbacher, M., Gysel-Beer, M., Kanji, Z.A., 2021. The contribution of Saharan dust to the ice-nucleating particle concentrations at the High Altitude Station Jungfraujoch (3580 m a.s.l.), Switzerland. Atmos. Chem. Phys. 21, 18029–18053. https://doi.org/10.5194/acp-21-18029-2021